

Cite this: *Nanoscale*, 2018, **10**, 791

# Upconverting nanocomposites with combined photothermal and photodynamic effects†

 Yue Huang,<sup>a</sup> Artiom Skripka,<sup>a</sup> Lucía Labrador-Páez,<sup>b</sup> Francisco Sanz-Rodríguez,<sup>b,c</sup> Patricia Haro-González,<sup>b</sup> Daniel Jaque,<sup>b,c</sup> Federico Rosei<sup>a,d,e</sup> and Fiorenzo Vetrone<sup>a,\*</sup>

Lanthanide-doped upconverting nanoparticles (UCNPs) have been studied for diverse biomedical applications due to their inherent ability to convert near-infrared (NIR) excitation light to higher energies (spanning the ultraviolet, visible, and NIR regions). To explore additional functionalities, rational combination with other optically active nanostructures may lead to the development of new multimodal nanoplateforms with theranostic (therapy and diagnostic) capabilities. Here, we develop a nanocomposite consisting of NaGdF<sub>4</sub>:Er<sup>3+</sup>, Yb<sup>3+</sup> UCNPs, mesoporous silica (SiO<sub>2</sub>), gold nanorods (GNRs) and a photosensitizer, with integrated functionalities including luminescence imaging, photothermal generation, nanothermometry and photodynamic effects. Under 980 nm irradiation, GNRs and UCNPs are simultaneously excited due to the overlap between the surface plasmon resonance of the GNRs and the absorption of the UCNPs leading to plasmonic enhancement of the upconverted luminescence, while concomitantly creating a temperature gradient. The temperature increase can be determined from the intensity ratio of the upconverted green emission of the UCNPs. Finally, a photosensitizer, zinc phthalocyanine, was loaded into the mesoporous SiO<sub>2</sub>. Upon laser irradiation, the upconverted visible light subsequently activates the photosensitizer to release reactive oxygen species. The multifunctional GNR@SiO<sub>2</sub>@UCNPs nanocomposites showed strong luminescence signal when incubated in HeLa cervical cancer cells, making them ideal bioprobes for future theranostic applications.

 Received 26th July 2017,  
 Accepted 3rd December 2017

DOI: 10.1039/c7nr05499h

rsc.li/nanoscale

## Introduction

In recent years, lanthanide (Ln<sup>3+</sup>)-doped upconverting nanoparticles (UCNPs) have been intensively investigated, largely focusing on potential applications such as nanoscale thermometry, diagnostics and therapy. In particular, significant research has focused on their use as multifunctional nanoscale platforms with combined therapeutic and diagnostic (theranostic) modalities.<sup>1–3</sup> The rising interest in UCNPs stems from their unorthodox excitation schemes where they can be

excited with near-infrared (NIR) light and ultimately emit higher energy photons spanning the ultraviolet (UV), visible and NIR regions *via* a multiphoton excitation process, known as upconversion.<sup>4–6</sup> The upconverted (or anti-Stokes) luminescence of UCNPs is advantageous when compared with conventional (Stokes) fluorescence from other nanomaterials, for several reasons. The NIR excitation light causes minimal photodamage, induces practically no autofluorescence background, and can penetrate biological tissues to a much greater extent.<sup>7,8</sup> As an added benefit, some of the upconverted Ln<sup>3+</sup> emission bands are sensitive to the surrounding temperatures, thereby allowing them to be effectively used as thermal nanoprobes (nanoscale thermometers also known as nanothermometers). One of the most well-known examples of an optical nanothermometer exploits the temperature sensitive emissions of the Er<sup>3+</sup> ion. In particular, the relative intensity of the two green emission bands emanating from the <sup>2</sup>H<sub>11/2</sub> and <sup>4</sup>S<sub>3/2</sub> excited states of Er<sup>3+</sup> change as a function of temperature. Consequently, Er<sup>3+</sup>-doped UCNPs have been used as non-contact, non-invasive optical nanothermometers to measure the temperature of living cells.<sup>9,10</sup>

In parallel to research on UCNPs, a significant body of work has focused on applying the heat generation capabilities of

<sup>a</sup>Institut National de la Recherche Scientifique (INRS), Centre Énergie, Matériaux et Télécommunications, Université du Québec, 1650 Boulevard Lionel-Boulet, Varennes, Québec J3X 1S2, Canada. E-mail: vetrone@emt.inrs.ca

<sup>b</sup>Fluorescence Imaging Group, Departamento de Física de Materiales, Facultad de Ciencias, Universidad Autónoma de Madrid, Madrid, 28049, Spain

<sup>c</sup>Instituto Ramón y Cajal de Investigación Sanitaria, Hospital Ramón y Cajal, Madrid, 28034, Spain

<sup>d</sup>Institute of Fundamental and Frontier Science, University of Electronic Science and Technology of China, Chengdu, 610051, China

<sup>e</sup>Centre for Self-Assembled Chemical Structures, McGill University, Montréal, H3A 2K6, Canada

†Electronic supplementary information (ESI) available: Supplementary figures. See DOI: 10.1039/c7nr05499h



Recently, additional functionalities could be attained from UCNPs through rational combination with other optically active nanostructures, resulting in promising multi-modal nanoplatforms combining therapeutic and diagnostic actions.<sup>28–30</sup> In this work, we developed a multifunctional nanocomposite based on the combination of UCNPs with GNRs, prepared through a layer-by-layer assembly. The GNR cores were coated

In a typical synthesis of the lanthanide trifluoroacetate precursors, 0.975 mmol (353.4 mg)  $\text{Gd}_2\text{O}_3$ , 0.025 mmol (9.6 mg, 2 mol% doping rate)  $\text{Er}_2\text{O}_3$ , and 0.25 mmol (98.5 mg, 20 mol% doping rate)  $\text{Yb}_2\text{O}_3$  were mixed in a 100 mL three-neck round-bottom flask with 5 mL distilled water and 5 mL trifluoroacetic acid, followed by refluxing under magnetic stirring at 80 °C until a clear solution was obtained. Subsequently, the temperature was reduced to 60 °C to evaporate the residual trifluoroacetic acid and water. The dried precursor was isolated in the form of a colorless powder.

## Nanoscale, 2018, 10, 791–799 | 793



mately 550 nm. The HeLa cells were mounted on a 0.1  $\mu\text{m}$  resolution XY stage such that it was possible to scan the HeLa cells with respect to the 980 nm laser spot.

### Characterization

The crystalline phase of all nanostructures under investigation was analyzed by X-ray diffraction (XRD, Bruker D8 Advanced Diffractometer, Cu  $K\alpha$  radiation). Dynamic light scattering (DLS, Malvern, Zetasizer Nano S90) was used to determine the hydrodynamic diameter of the nanostructures. The morphology and size distribution of the GNRs and UCNPs were determined with a Philips CM200 high-resolution transmission electron microscope (HR-TEM), equipped with an energy-dispersive X-ray (EDX) unit. The UV-Visible (UV-VIS) absorption spectra were obtained using a UV-VIS spectrometer (Varian Cary 5000). Luminescent measurements were carried out under 980 nm excitation using a laser diode (Thorlabs fiber-coupled laser 305 diode). The laser beam was focused on the sample using a lens to obtain a spot with a Gaussian intensity distribution with a 0.4 mm diameter. The emitted light was collected by a lens in a 90° configuration, and then transferred to a spectrophotometer (Avaspec-2048L-USB2) using an optical fiber.

## Results and discussion

### Preparation and characterization of GNR@SiO<sub>2</sub>@UCNPs

To prepare the multifunctional nanocomposites based on UCNPs and GNRs with combined luminescence, photodynamic and photothermal properties for potential use in theranostics, a layer-by-layer procedure was employed. This multifunctional nanocomposite contains a mesoporous SiO<sub>2</sub> layer separating the UCNPs decorated on the surface and the GNR core, which has multiple roles. First, it is used as a scaffold for the attachment of the UCNPs. Second, it acts as a spacer to separate the plasmonic nanostructure (GNR) and the fluorescent species (UCNPs) leading to minimal luminescence quenching and potentially, plasmonic enhancement. Finally, the pores can be loaded with photosensitizer molecules capable of transforming the upconverted visible radiation to ROS (*i.e.*  $^1\text{O}_2$ ) adding another modality to the nanoplatform. To prepare this nanocomposite, a multistep synthetic method was proposed and summarized in Scheme 1. Initially, the NaGdF<sub>4</sub>:Er<sup>3+</sup>, Yb<sup>3+</sup> UCNPs were synthesized by the previously described thermal decomposition method.<sup>37</sup> As seen in Fig. 1A, the synthesized UCNPs were monodisperse and uniform with an average dia-

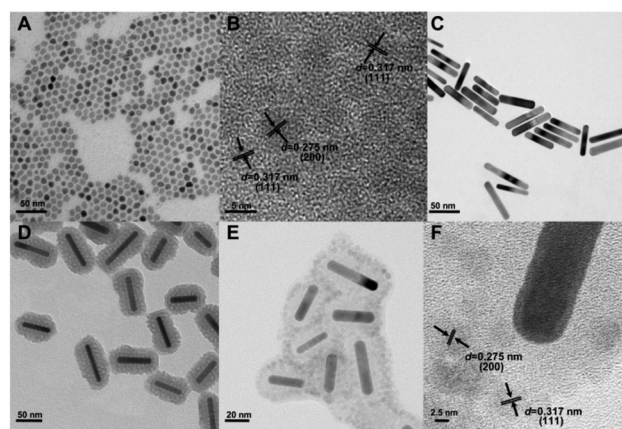


**Fig. 1** (A) TEM and (B) HR-TEM images of the synthesized NaGdF<sub>4</sub>:Er<sup>3+</sup>, Yb<sup>3+</sup> UCNPs. TEM images of the (C) synthesized GNRs, (D) the SiO<sub>2</sub> coated GNRs (GNR@SiO<sub>2</sub>), and (E) the hybrid SiO<sub>2</sub> coated GNRs decorated with NaGdF<sub>4</sub>:Er<sup>3+</sup>, Yb<sup>3+</sup> UCNPs (GNR@SiO<sub>2</sub>@UCNPs), (F) HR-TEM image of the GNR@SiO<sub>2</sub>@UCNPs interface.

meter of approximately 6.5 nm. The HR-TEM image of the UCNPs is shown in the Fig. 1B and the lattice fringes were clearly observed with a spacing of  $\sim 0.275$  nm,  $\sim 0.317$  nm assigned to the {200}, {111} planes of cubic ( $\alpha$ -) phase NaGdF<sub>4</sub>:Er<sup>3+</sup>, Yb<sup>3+</sup> UCNPs, respectively. This result is consistent with XRD studies (Fig. 2B), which confirmed that the UCNPs crystallized in the  $\alpha$ -phase, and no impurity crystalline phase was found in the diffraction pattern. Separately, GNRs were prepared according to a previously published protocol<sup>38</sup> and their morphology and average size were imaged by TEM (Fig. 1C). GNRs with an average of 72 nm in length and 12 nm in diameter were successfully synthesized, yielding an aspect ratio of

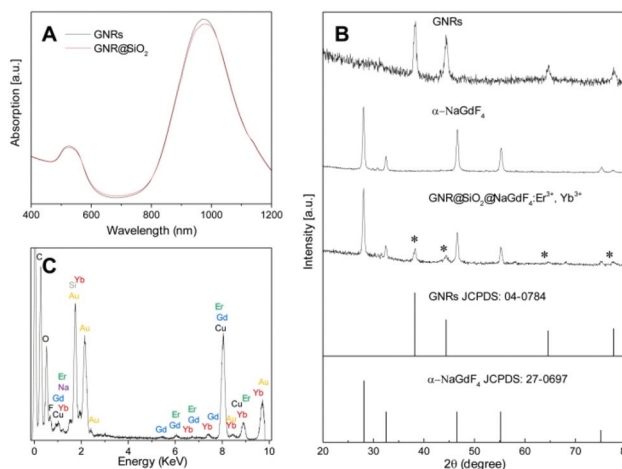


**Fig. 2** (A) Extinction spectra of GNRs and GNR@SiO<sub>2</sub>. (B) XRD patterns of GNRs,  $\alpha$ -NaGdF<sub>4</sub>:Er<sup>3+</sup>, Yb<sup>3+</sup>, hybrid nanocomposite of GNRs and NaGdF<sub>4</sub>:Er<sup>3+</sup>, Yb<sup>3+</sup> (GNR@SiO<sub>2</sub>@UCNPs). The standard pattern of pure GNRs (JCPDS file No: 04-0784), pure  $\alpha$ -NaGdF<sub>4</sub> (JCPDS file No: 27-0697) are provided for reference. The stars show the diffraction peaks of GNRs in the GNR@SiO<sub>2</sub>@UCNPs nanocomposite. (C) Elemental analysis of hybrid GNRs@SiO<sub>2</sub>@UCNPs nanocomposite by EDX.



**Scheme 1** Schematic illustration of the synthetic procedure for the preparation of the GNR@SiO<sub>2</sub>@UCNPs nanocomposite.





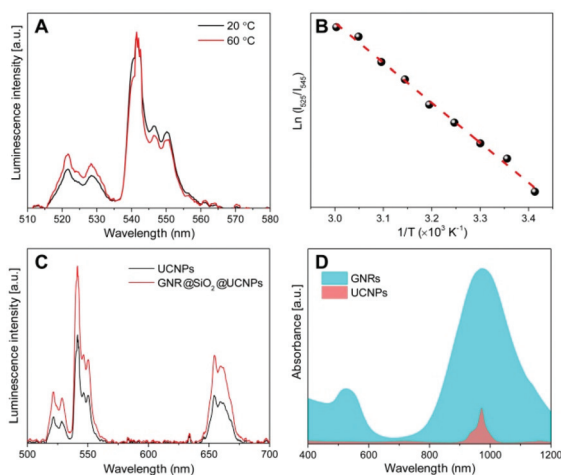


**Fig. 3** (A) Normalized upconversion luminescence spectra of UCNPs at two different temperatures. (B) The temperature dependence of the ratio calculated from the luminescence spectra obtained at various temperatures. Dots are experimental results and the red line is the best linear fit. (C) Upconversion luminescence spectra of UCNPs and GNR@SiO<sub>2</sub>@UCNPs. (D) Normalized absorption spectra of UCNPs and GNRs.

515–535 nm and 535–570 nm emissions of the GNR@SiO<sub>2</sub>@UCNPs nanocomposite clearly increases when compared with that of the bare UCNPs at the same conditions. The thermal change of the GNR@SiO<sub>2</sub>@UCNPs nanocomposites under NIR excitation was determined by the previously obtained linear regression equation for the NaGdF<sub>4</sub>:Er<sup>3+</sup>, Yb<sup>3+</sup> UCNPs. Under NIR excitation of 0.8 W the temperature in the excitation area of 0.4 mm in diameter, changed by approximately 1.0 and 7.3 °C for UCNPs alone and GNR@SiO<sub>2</sub>@UCNPs nanocomposites, respectively (Fig. S4†). In turn, this shows that the UCNPs attached to the surface of GNRs can be successfully used for real-time temperature sensing at the nanoscale, particularly for precise control of photothermal effect. Meanwhile, it is worth noting that the nanocomposites are quite stable after laser excitation, since the same luminescence intensity and heating properties could be observed after several cycles of laser irradiation, which demonstrates that UCNPs are not lost from the surface of GNR@SiO<sub>2</sub> and no morphological changes occur to the GNRs (they retain their rod-like morphology). In this nanocomposite, the GNRs could therefore easily be used as nanoscale heaters when excited at 980 nm, while the UCNPs decorated on the surface of the SiO<sub>2</sub> shell effectively behave as thermal sensors. Moreover, the total emission from the Er<sup>3+</sup> ions in the GNR@SiO<sub>2</sub>@UCNPs nanocomposite was enhanced when compared with bare UCNPs. This is due to the fact that when the SPR of the GNRs overlaps with the excitation of the UCNPs (<sup>2</sup>F<sub>5/2</sub> from Yb<sup>3+</sup> and <sup>4</sup>I<sub>11/2</sub> from Er<sup>3+</sup> at 980 nm), as shown in Fig. 3D, the energy harnessed by the plasmonic nanostructures (GNRs) could be transferred to the electrons of the Ln<sup>3+</sup> dopants in the UCNPs, resulting in an increase in their absorption cross-section.<sup>25,41</sup> Further to this, the SPR can affect the

upconversion luminescence depending on the relative position of the SPR from the excitation or emission of UCNPs as well as the distance separating the UCNPs from the metal surface, that is to say, the thickness of the spacer layer between the UCNPs and the surface of the GNRs.<sup>42</sup> There are three competitive effects that contribute to this behavior: the plasmonic field causing luminescence enhancement, the radiative decay rate from coupling of the upconversion emission with the SPR of the GNRs resulting in luminescence enhancement and the non-radiative energy transfer resulting in luminescence quenching. In this study, the SPR (980 nm) of the GNRs was far away from the upconversion emission, therefore, the radiative decay rate played a negligible role. If the fluorescent species (UCNPs) are close to the metal surface, the upconversion luminescence decreases, as the non-radiative energy transfer is dominant. With the increase of the distance between the two species (*i.e.* the thickness of the spacer layer in this case SiO<sub>2</sub>), the plasmonic field enhancement becomes dominant leading to the observed increase of the UCNPs luminescence.

#### Characterization of ZnPc loaded GNR@SiO<sub>2</sub>@UCNPs and photodynamic effect

The photosensitizer ZnPc was selected as candidate to be loaded into the mesoporous silica and to deliver the desired photodynamic effect. A concentrated solution of ZnPc was mixed together with the GNR@SiO<sub>2</sub>@UCNPs until the ZnPc was absorbed into the porous SiO<sub>2</sub>. The ZnPc loading capacity was determined by the UV-VIS spectra and reached 1.8% (w/w). Meanwhile, the luminescence intensity of ZnPc loaded GNR@SiO<sub>2</sub>@UCNPs under NIR laser irradiation was also investigated and it was observed that a quenching of the luminescence occurred after ZnPc was loaded into the GNR@SiO<sub>2</sub>@UCNPs nanocomposite (Fig. 4A). In fact, the red emission (<sup>4</sup>F<sub>9/2</sub> → <sup>4</sup>I<sub>15/2</sub>) of the GNR@SiO<sub>2</sub>@UCNPs from Er<sup>3+</sup> decreased by 54%, which was significantly more than the decrease in green emission (29%). This quenching resulted from efficient energy transfer between the UCNPs (energy donors) and the ZnPc molecules (energy acceptors) due to the favorable spectral overlap between the red emission of the UCNPs at 660 nm and the absorption of ZnPc at 665 nm (Fig. 4B). In addition, the ratio of the green emission bands discussed above remains almost unchanged after ZnPc loading in the GNR@SiO<sub>2</sub>@UCNPs nanocomposites indicating that the LIR technique can still be used for thermal sensing after loading.

The capacity of ROS production, in particular singlet oxygen (<sup>1</sup>O<sub>2</sub>), was assessed using ABDA as a probe molecule. As shown in Fig. 4C, three control groups were studied, ABDA incubated with ZnPc loaded GNR@SiO<sub>2</sub>@UCNPs without NIR laser irradiation (blue triangles), ZnPc molecules with NIR laser irradiation (black squares), and GNR@SiO<sub>2</sub>@UCNPs alone with NIR laser irradiation (red circles). No significant changes are observed for these control groups over time, which indicates that no <sup>1</sup>O<sub>2</sub> generation occurred. However, for ABDA incubated with ZnPc loaded GNR@SiO<sub>2</sub>@UCNPs follow-





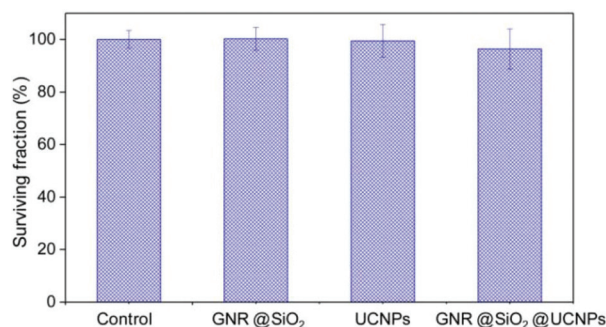


**Fig. 4** (A) Upconversion luminescence spectra of GNR@SiO<sub>2</sub>@UCNPs and ZnPc loaded GNR@SiO<sub>2</sub>@UCNPs under 980 nm laser irradiation. (B) Upconversion emission spectrum of NaGdF<sub>4</sub>:Er<sup>3+</sup>, Yb<sup>3+</sup> UCNPs and UV-VIS absorption spectrum of ZnPc, indicating the partial spectral overlap between the ZnPc absorption and the UCNP emission. (C) Production of <sup>1</sup>O<sub>2</sub> under consumption of ABDA for different samples over time. (D) Production of <sup>1</sup>O<sub>2</sub> under consumption of ABDA in the absence and presence of laser irradiation.

uted to the positively APTES capped GNR@SiO<sub>2</sub> nanostructures, which could lead to the cellular cytotoxicity in terms of causing mitochondrial and lysosomal damage.<sup>43,44</sup>

Once the low cytotoxicity of the multifunctional platforms was evidenced, we proceeded with cell imaging studies. In doing so, HeLa cells were incubated with a solution containing the GNR@SiO<sub>2</sub>@UCNPs nanocomposites. Incubation time was set to 24 h. After incubation, cells were washed and placed in the confocal microscope. The 980 nm focal plane was set to match the axial location of the HeLa cells and these were scanned while recording the emission spectra in the 500–580 nm spectral range. A typical bright field (BF) optical image of an individual HeLa cell is included in Fig. 6A. The spatial variation of the green fluorescence intensity obtained when the 980 nm laser was scanned over the HeLa cell of Fig. 6A is shown in Fig. 6B. When both fluorescence and BF optical images are merged (see Fig. 6C) it is clear that the GNR@SiO<sub>2</sub>@UCNPs nanocomposites are incorporated within the HeLa cell since the luminescence signal is very well localized inside the cell. This suggests that the GNR@SiO<sub>2</sub>@UCNPs nanocomposites have been accumulated at a well-defined location inside the cell. This is in good agreement with previous

**Fig. 6** (A) BF optical image of a HeLa cancer cell incubated for a period of 24 h with GNR@SiO<sub>2</sub>@UCNPs. (B) Fluorescence image obtained by scanning the 980 nm laser spot over the HeLa cell in (A) and by recording the emitted intensity in the 500–580 nm spectral range. (C) Merge of optical and fluorescence images denoting accumulation of GNR@SiO<sub>2</sub>@UCNPs inside the HeLa cell. (D) Emission spectra as obtained at two different locations inside the cell denoted by green and black arrows in (C). (E), (F), and (G) are the BF optical image, micro-luminescence map, and merged image of a HeLa cell for control, respectively. Scale bars: 10  $\mu$ m.

work.<sup>45</sup> It has been stated that agglomeration of UCNPs inside HeLa cells could take place for long incubation times (as in our case). This effect is a consequence of the intracellular transportation of nutrients from the cellular membrane to the Golgi apparatus. To verify that the green emission collected was generated by the GNR@SiO<sub>2</sub>@UCNPs nanocomposites, the emission spectra were recorded at two different locations inside the HeLa cell. Results are shown in Fig. 6D. When compared with the emission spectra included in Fig. 3 and 4, it is clearly observed that the fluorescence image was generated by the GNR@SiO<sub>2</sub>@UCNPs nanocomposites. Control experiments, by using HeLa cells incubated in a medium dispersion without GNR@SiO<sub>2</sub>@UCNPs nanocomposites were also conducted, revealing the complete absence of fluorescence contrast (see Fig. 6E–G).

## Conclusions

In summary, a GNR@SiO<sub>2</sub>@UCNPs nanocomposite was synthesized and characterized. We studied the photothermal generation as well as the luminescence properties of the GNR@SiO<sub>2</sub>@UCNPs and observed that after NIR excitation at 980 nm, significant heating was produced from the plasmonic GNRs at the core of the nanocomposite. It was determined that the ratio of the intensities of the green upconverted emission between the <sup>2</sup>H<sub>11/2</sub> → <sup>4</sup>I<sub>15/2</sub> and <sup>4</sup>S<sub>3/2</sub> → <sup>4</sup>I<sub>15/2</sub> transitions from the UCNPs functionalized on the surface of the mesoporous SiO<sub>2</sub> shell surrounding the GNR cores changed as a function of temperature and could be exploited for thermal sensing resulting in a nanocomposite with both photothermal generation capabilities and real time temperature monitoring. Moreover, the total luminescence intensity of the UCNPs was increased in the presence of GNRs (compared to the UCNPs alone) and this enhancement was attributed to the overlap of the excitation of the UCNPs with the SPR of the GNRs at 980 nm as well to the mesoporous SiO<sub>2</sub> between the UCNPs and GNR acting as a spacer to mitigate any non-radiative energy transfer between the plasmonic GNR and the luminescent UCNPs. Thus, the luminescence of the UCNPs was influenced by the localized electromagnetic field created by the GNRs, which leads to the observed enhancement in the luminescence intensity. ZnPc was selected as a photosensitizer to load into the mesoporous SiO<sub>2</sub> layer and a quenching of the UCNPs was observed following loading of the pores. This demonstrated that the emitted upconverted luminescence was effectively absorbed by the ZnPc molecules, which subsequently generated the ROS. Finally, *in vitro* cell experiments were performed to assess the cytotoxicity of GNRs@SiO<sub>2</sub>@UCNPs. Results showed the absence of any cytotoxicity on the incubated cells thus determining that they were excellent biocompatible nanocomposites. Similarly, cell labeling experiments were performed and it was determined that the GNR@SiO<sub>2</sub>@UCNPs nanocomposites accumulated at a well-defined location inside the HeLa cells and were imaged *via* the upconverted green luminescence from inside the cells. These

results confirm that GNR@SiO<sub>2</sub>@UCNPs have the potential to be used as NIR-excited multifunctional nanoplateforms for theranostic applications, specifically due to their photothermal and photodynamic capabilities.

## Conflicts of interest

There are no conflicts to declare.

## Acknowledgements

F. V. and F. R. acknowledge funding from the Natural Sciences and Engineering Research Council (NSERC Discovery Grants) of Canada and Fonds de Recherche du Québec-Nature et technologies (FRQNT) for supporting this research. F. V. also is grateful to the Fondation Sibylla Hesse for funding. Y. H. acknowledges financial support from the Merit Scholarship Program for Foreign Students from the Ministère de l'Éducation, du Loisir et du Sport du Québec. F. R. is grateful to the Canada Research Chairs program for partial salary support and acknowledges NSERC for an EWR Steacie Memorial Fellowship. F. R. is also grateful to the Government of China for a Chang Jiang Scholar Short Term Award and to Sichuan Province for a 1000 talent short term award. L. L.-P., P. H.-G., and D. J. acknowledge the Spanish Ministerio de Educación y Ciencia (MAT2013-47395-C4-1-R and MAT2016-75362-C3-1-R) and the EU Framework Programme (COST Action CM1403) for supporting this research. L. L.-P. also thanks the Universidad Autónoma de Madrid for the "Formación de Personal Investigador (FPI-UAM)" program. P. H.-G. is grateful to the Spanish Ministerio de Economía y Competitividad (MINECO) for the Juan de la Cierva program.

## Notes and references

- 1 J. Zhou, Q. Liu, W. Feng, Y. Sun and F. Y. Li, *Chem. Rev.*, 2015, **115**, 395–465.
- 2 G. Y. Chen, H. L. Qiu, P. N. Prasad and X. Y. Chen, *Chem. Rev.*, 2014, **114**, 5161–5214.
- 3 F. Wang, D. Banerjee, Y. S. Liu, X. Y. Chen and X. Liu, *Analyst*, 2010, **135**, 1839–1854.
- 4 F. Auzel, *Chem. Rev.*, 2004, **104**, 139–174.
- 5 H. Dong, L. D. Sun and C. H. Yan, *Nanoscale*, 2013, **5**, 5703–5714.
- 6 J. A. Capobianco, F. Vetrone, T. D'Alesio, G. Tessari, A. Speghini and M. Bettinelli, *Phys. Chem. Chem. Phys.*, 2000, **2**, 3203–3207.
- 7 J. Zhou, Z. Liu and F. Y. Li, *Chem. Soc. Rev.*, 2012, **41**, 1323–1349.
- 8 E. Hemmer, A. Benayas, F. Légaré and F. Vetrone, *Nanoscale Horiz.*, 2016, **1**, 168–184.
- 9 F. Vetrone, R. Naccache, A. Zamarron, A. J. de la Fuente, F. Sanz-Rodriguez, L. M. Maestro, E. M. Rodriguez,





- 3 D. Jaque, J. G. Sole and J. A. Capobianco, *ACS Nano*, 2010, **4**, 3254–3258.
- 4 D. Jaque and F. Vetrone, *Nanoscale*, 2012, **4**, 4301–4326.
- 5 D. Jaque, L. Martínez Maestro, B. del Rosal, P. Haro-Gonzalez, A. Benayas, J. L. Plaza, E. Martín Rodríguez and J. García Solé, *Nanoscale*, 2014, **6**, 9494–9530.
- 6 L. Cheng, C. Wang, L. Z. Feng, K. Yang and Z. Liu, *Chem. Rev.*, 2014, **14**, 10869–10939.
- 7 C. D. Brites, P. P. Lima, N. J. O. Silva, A. Millán, V. S. Amaral, F. Palacio and L. D. Carlos, *Nanoscale*, 2012, **4**, 4799–4829.
- 8 P. K. Jain, X. H. Huang, I. H. El-Sayed and M. A. El-Sayed, *Acc. Chem. Res.*, 2008, **41**, 1578–1586.
- 9 N. S. Abadeer and C. J. Murphy, *J. Phys. Chem. C*, 2016, **120**, 4691–4716.
- 10 A. M. Alkilany, L. B. Thompson, S. P. Boulos, P. N. Sisco and C. J. Murphy, *Adv. Drug Delivery Rev.*, 2012, **64**, 190–199.
- 11 X. H. Huang, S. Neretina and M. A. El-Sayed, *Adv. Mater.*, 2009, **21**, 4880–4910.
- 12 Z. J. Zhang, J. Wang and C. Y. Chen, *Theranostics*, 2013, **3**, 223–238.
- 13 G. Baffou, R. Quidant and C. Girard, *Appl. Phys. Lett.*, 2009, **94**, 153109.
- 14 A. M. Alkilany, P. K. Nagaria, C. R. Hexel, T. J. Shaw, C. J. Murphy and M. D. Wyatt, *Small*, 2009, **5**, 701–708.
- 15 E. Locatelli, I. Monaco and M. C. Franchini, *RSC Adv.*, 2015, **5**, 21681–21699.
- 16 Z. J. Zhang, L. M. Wang, J. Wang, X. M. Jiang, X. H. Li, Z. J. Hu, Y. H. Ji, X. C. Wu and C. Y. Chen, *Adv. Mater.*, 2012, **24**, 1418–1423.
- 17 S. Shen, H. Y. Tang, X. T. Zhang, J. F. Ren, Z. Q. Pang, D. G. Wang, H. L. Gao, Y. Qian, X. G. Jiang and W. L. Yang, *Biomaterials*, 2013, **34**, 3150–3158.
- 18 A. J. Gormley, N. Larson, S. Sadekar, R. Robinson, A. Ray and H. Ghandehari, *Nano Today*, 2012, **7**, 158–167.
- 19 W. Park, D. Lu and S. Ahn, *Chem. Rev.*, 2015, **44**, 2940–2962.
- 20 F. Zhang, G. B. Braun, Y. F. Shi, Y. C. Zhang, X. H. Sun, N. O. Reich, D. Y. Zhao and G. Stucky, *J. Am. Chem. Soc.*, 2010, **132**, 2850–2851.
- 21 W. Ge, X. R. Zhang, M. Liu, Z. W. Lei, R. J. Knize and Y. L. Lu, *Theranostics*, 2013, **3**, 282–288.
- 22 R. Lv, P. Yang, B. Hu, J. Xu, W. Shang and J. Tian, *ACS Nano*, 2017, **11**, 1064–1072.
- 23 A. Skripka, R. Marin, A. Benayas, P. Canton, E. Hemmer and F. Vetrone, *Phys. Chem. Chem. Phys.*, 2017, **19**, 11825–11834.
- 24 R. Lv, P. Yang, F. He, S. Gai, G. Yang, Y. Dai, Z. Hou and J. Lin, *Biomaterials*, 2015, **63**, 115–127.
- 25 G. Valduga, E. Reddi, S. Garbisa and G. Jori, *Int. J. Cancer*, 1998, **75**, 412–417.
- 26 C. N. Zhou, S. J. Chi, J. S. Deng, J. L. Liang, G. Jori and C. Milanese, *J. Photochem. Photobiol., B*, 1996, **33**, 219–223.
- 27 Y. Huang, E. Hemmer, F. Rosei and F. Vetrone, *J. Phys. Chem. B*, 2016, **120**, 4992–5001.
- 28 B. Nikoobakht and M. A. El-Sayed, *Chem. Mater.*, 2003, **15**, 1957–1962.
- 29 T. Zhao, H. Wu, S. Q. Yao, Q. H. Xu and G. Q. Xu, *Langmuir*, 2010, **26**, 14937–14942.
- 30 F. Denizot and R. Lang, *J. Immunol. Methods*, 1986, **89**, 271–277.
- 31 H. X. Mai, Y. W. Zhang, R. Si, Z. G. Yan, L. D. Sun, L. P. You and C. H. Yan, *J. Am. Chem. Soc.*, 2006, **128**, 6426–6436.
- 32 X. Ye, L. Jin, H. Caglayan, J. Chen, G. Xing, C. Zheng, V. Doan-Nguyen, Y. Kang, N. Engheta, C. R. Kagan and C. B. Murray, *ACS Nano*, 2012, **6**, 2804–2817.
- 33 I. Gorelikov and N. Matsuura, *Nano Lett.*, 2008, **8**, 369–373.
- 34 Y. Huang, F. Rosei and F. Vetrone, *Nanoscale*, 2015, **7**, 5178–5185.
- 35 M. Saboktakin, X. C. Ye, U. K. Chettiar, N. Engheta, C. B. Murray and C. R. Kagan, *ACS Nano*, 2013, **7**, 7186–7192.
- 36 M. Saboktakin, X. Ye, S. J. Oh, S. H. Hong, A. T. Fafarman, U. K. Chettiar, N. Engheta, C. B. Murray and C. R. Kagan, *ACS Nano*, 2012, **6**, 8758–8766.
- 37 E. Frohlich, *Int. J. Nanomed.*, 2012, **7**, 5577–5591.
- 38 S. Bhattacharjee, L. H. J. de Haan, N. M. Evers, X. Jiang, A. T. M. Marcelis, H. Zuilhof, I. M. C. M. Rietjens and G. M. Alink, *Part. Fibre Toxicol.*, 2010, **7**, 25.
- 39 F. Vetrone, R. Naccache, A. J. de la Fuente, F. Sanz-Rodriguez, A. Blazquez-Castro, E. M. Rodriguez, D. Jaque, J. G. Sole and J. A. Capobianco, *Nanoscale*, 2010, **2**, 495–498.

